

## Phonon Thermal Transport in $\text{UO}_2$ via Self-Consistent Perturbation Theory

Shuxiang Zhou<sup>1</sup>, Enda Xiao<sup>2</sup>, Hao Ma<sup>3,4</sup>, Krzysztof Gofryk<sup>1</sup>, Chao Jiang<sup>1</sup>,

Michael E. Manley<sup>3</sup>, David H. Hurley<sup>1</sup>, and Chris A. Marianetti<sup>5</sup>

<sup>1</sup>Idaho National Laboratory, Idaho Falls, Idaho 83415, USA

<sup>2</sup>Department of Chemistry, Columbia University, New York, New York 10027, USA

<sup>3</sup>Oak Ridge National Laboratory, Oak Ridge, Tennessee 37831, USA

<sup>4</sup>Department of Thermal Science and Energy Engineering, University of Science and Technology of China, Hefei, Anhui 230026, China

<sup>5</sup>Department of Applied Physics and Applied Mathematics, Columbia University, New York, New York 10027, USA



(Received 13 October 2023; revised 17 January 2024; accepted 12 February 2024; published 6 March 2024)

Computing thermal transport from first-principles in  $\text{UO}_2$  is complicated due to the challenges associated with Mott physics. Here, we use irreducible derivative approaches to compute the cubic and quartic phonon interactions in  $\text{UO}_2$  from first principles, and we perform enhanced thermal transport computations by evaluating the phonon Green's function via self-consistent diagrammatic perturbation theory. Our predicted phonon lifetimes at  $T = 600$  K agree well with our inelastic neutron scattering measurements across the entire Brillouin zone, and our thermal conductivity predictions agree well with previous measurements. Both the changes due to thermal expansion and self-consistent contributions are nontrivial at high temperatures, though the effects tend to cancel, and interband transitions yield a substantial contribution.

DOI: [10.1103/PhysRevLett.132.106502](https://doi.org/10.1103/PhysRevLett.132.106502)

Uranium dioxide ( $\text{UO}_2$ ) has attracted a great deal of research interest since the 1950s, both as a standard nuclear fuel and as a fundamental system of rich physics induced by the partially filled  $f$  shell [1,2]. As thermal transport is critical in nuclear fuels, phonon thermal transport in  $\text{UO}_2$  has been extensively studied both by experiments [3–7] and from first principles [8–14]. However, wide-ranging results were obtained from first-principles computations, and a robust consensus has not yet merged (see Sec. II in Supplemental Material (SM) [15] for a detailed discussion of the different approaches). While low-temperature thermal conductivity is substantially complicated by magnons, defects, and boundary effects, room temperature and beyond should be dominated by phonon thermal transport. However, accurately computing phonon interactions in  $\text{UO}_2$  from first principles is complicated due to the complex interplay of Mott physics, magnetic order, and spin-orbit coupling (SOC). Here, we circumvent these technical challenges by employing  $f$ -orbital occupation matrix control [26–29] and the  $3k$  antiferromagnetic ground state obtained by our previous study [30], which provides a robust description of the ground state and phonons as compared to experiment.

Phonon thermal conductivity has been reliably computed in band insulators by solving the linearized phonon Peierls-Boltzmann transport equation (BTE) from first principles using scattering rates computed within leading order perturbation theory [31–34]. This *de facto* standard approach for computing phonon thermal conductivity, as

implemented by multiple publicly available software packages [35–38], solves the BTE using cubic phonon interactions and the imaginary part of the bare bubble diagram. Naturally, nontrivial inaccuracy will occur under extreme conditions (e.g., high temperatures) where perturbation theory is inadequate. More recently, quartic phonon interactions have been incorporated using the imaginary part of the sunset diagram [39,40], and the contribution of interband phonon transitions has been addressed by a generalization of the BTE, known as the Wigner transport equation (WTE) [41,42]. Here, we go beyond the current state of the art for computing thermal conductivity, which only uses the imaginary parts of the bubble and sunset diagrams, by using self-consistent diagrammatic perturbation theory to compute the single phonon Green's function [43].

In the present work, we use density functional theory plus  $U$  (DFT +  $U$ ) [44] to compute the cubic and quartic phonon interactions, which are then used to compute the inelastic neutron scattering (INS) function and thermal conductivity. Both the scattering function and the thermal conductivity are computed using increasingly sophisticated levels of theory, including bare perturbation theory and self-consistent perturbation theory [43]. For the latter, two different levels of self-consistency are employed: the Hartree-Fock (HF) approximation for phonons and quasiparticle perturbation (QP) theory. The former is the traditional variational approach of Hooton [45], where the four phonon loop diagram is evaluated self-consistently, and the

latter self-consistently evaluates both the four phonon loop diagram and the real part of the three phonon bubble diagram [43]. Following Ref. [43], the self-consistency scheme and the subsequent diagrams evaluated to construct the phonon self-energy are indicated by the notation  $\mathcal{S}_{ijk\dots}^A$ , where  $A \in \{o, HF, QP\}$  labels the self-consistency scheme and  $i, j, k, \dots$  indicate all diagrams evaluated post self-consistency (see Fig. 1 and S1 of Ref. [43] for schematics of diagrams). The colloquial diagram names bubble, loop, and sunset are abbreviated as  $b$ ,  $l$ , and  $s$ , respectively, while the self-consistency schemes  $o$ ,  $HF$ , and  $QP$  correspond to the bare, Hartree-Fock, and quasiparticle Green's function, respectively. For example, the imaginary part of the phonon self-energy used in the standard thermal conductivity approach [32] is obtained from  $\mathcal{S}_b^o$ ; and the approach in Ref. [40], which employs quartic phonon interactions using the imaginary part of the sunset diagram, is obtained from  $\mathcal{S}_{bs}^o$ . For each scheme we employ, both BTE and WTE are applied within the relaxation time approximation. For  $\mathcal{S}_b^o$ , the full solution to the BTE is also obtained, yielding results very close to the relaxation time approximation (see Sec. III of SM [15]), as is consistent with previous results for  $\text{ThO}_2$  [46] and  $\text{CaF}_2$  [46,47]. To include the effects of the thermal expansion, the phonons and phonon interactions are computed at three expanded volumes, according to the experimental thermal expansion coefficients at  $T = 360, 600, \text{ and } 1000 \text{ K}$  [48]. These computed results are linearly interpolated or extrapolated to temperatures from 0 to 1400 K.

Our DFT +  $U$  calculations were carried out using the projector augmented-wave method [49,50], as implemented in the Vienna *ab initio* simulation package code [51,52]. The exchange correlation functional employed in our DFT +  $U$  calculations was the generalized gradient approximation (GGA) as formulated by Perdew, Burke, and Ernzerhof [53], due to its overall better accuracy for phonons in  $\text{UO}_2$  (see Sec. IX of SM [15]). We used the rotationally invariant DFT +  $U$  approach of Dudarev *et al.* [54], which only employs a single effective interaction, and  $U = 4 \text{ eV}$  was used throughout. SOC was included in all calculations. We customized the Vienna *ab initio* simulation package code to initialize and monitor the occupation matrices during the calculations [30], and the initial values of the occupation matrices were taken from our previous work (i.e.,  $\mathbb{S}_0$ ) [30]. The cubic and quartic phonon interactions were calculated via the bundled irreducible derivative approach [55]. More information on the phonon interaction calculations, including supercell size,  $k$ -point mesh, and Born effective charges, is provided in Sec. III of SM [15]. Details of the thermal conductivity calculations are also provided in Sec. III of SM [15].

The scattering function  $S(\mathbf{Q}, \omega)$  at  $T = 600 \text{ K}$  was measured using the angular range chopper spectrometer (ARCS) with an incident neutron energy  $E_i = 120 \text{ meV}$  and ARCS-100-1.5-AST Fermi chopper [56]. Further

details of the  $\text{UO}_2$  crystal and ARCS measurements have been reported previously [57]. The ARCS energy resolution functions [56] were used in fitting the phonon peaks, and the reported widths are the intrinsic full-width half-maximum (FWHM) values that have been corrected for the instrument contribution. The ARCS instrument measures a large volume in  $Q$  and  $E$ , which contains many Brillouin zones, and the data analysis allows for an adjustable size of  $q$  voxel, a finite volume in reciprocal space associated with some  $q$  point, in all crystallographic directions. The  $q$ -voxel size is normally chosen to be as small as possible, with the minimum being dictated by having sufficient counting statistics, and the resulting scattering function is normally inherently broadened due to this issue [46]. To make a meaningful comparison against experiment, the usage of the experimental  $q$  voxel must be accounted for within theory. Details of the computation are reported in Ref. [46], and the  $q$ -voxel information is included in Sec. V of SM [15].

We begin by considering the INS scattering function, which was measured at  $T = 600 \text{ K}$ . The scattering function can be decomposed into components from  $n$ -phonon contributions, and the dominant peaks in the spectra arise from the one phonon contributions. The one phonon scattering function can be obtained from the phonon self-energy, which can be computed using standard tools from many-body physics [46]. Given that  $T = 600 \text{ K}$  is still a modest temperature, we will demonstrate that the bare bubble and loop diagrams are still sufficient to reasonably capture the INS scattering function peak width.

We begin by plotting the phonon linewidths computed using  $\mathcal{S}_b^o$ , which are overlaid on the phonon dispersion [see Fig. 1(a)]. The branch naming convention follows Ref. [58]. Generally, the acoustic branches have a much smaller FWHM than the optical branches, as is expected. For the INS scattering function, we first consider the particular example of  $\mathbf{Q} = [0.6, 0.6, 6.6]$ , where we individually illustrate the effects of the  $q$  voxel and energy resolution [see Fig. 1(b)]. The peak at approximately 12 meV corresponds to the transverse acoustic mode, whereas the longitudinal acoustic mode at approximately 20 meV is barely observable due to the weighting factors in the scattering function. Clearly, both the  $q$  voxel and energy resolution must be considered to make a meaningful comparison with INS measurements. The favorable agreement suggests that the level of theory we are using is robust, but a detailed comparison across the entire Brillouin zone is still needed.

We now proceed to comprehensively compare the computational and experimental results for the FWHMs of the scattering function peaks across the Brillouin zone (see Fig. 2). Following standard INS conventions, the energy resolution is removed from the peak width, and the theoretical results are presented for both the  $q$  point and the  $q$  voxel that was used in INS. Overall, there is favorable agreement across all modes and  $q$  paths, indicating that the

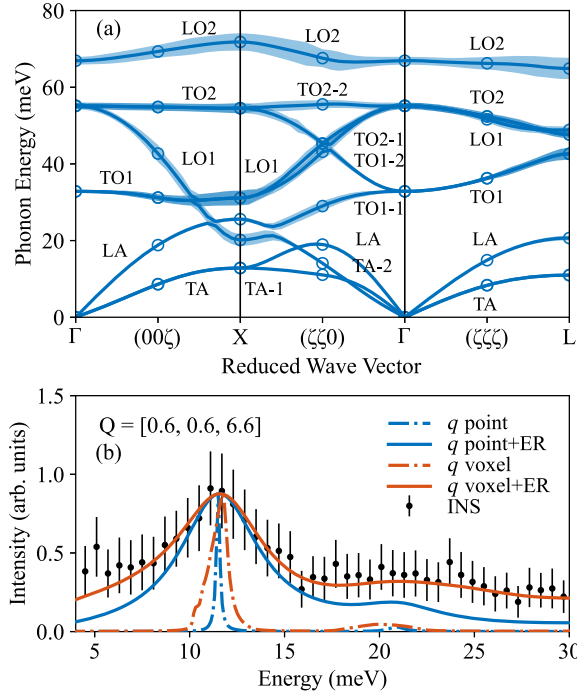


FIG. 1. (a) The unfolded phonon dispersion at  $T = 0$  K, computed using GGA +  $U$  + SOC ( $U = 4$  eV) in the  $3\mathbf{k}$  anti-ferromagnetic state. The hollow points were directly computed using DFT, while the corresponding curves are Fourier interpolations. The width of the line shading represents the FWHM computed at  $T = 600$  K using  $S_{ib}^o$ . (b)  $S(\mathbf{Q}, \omega)$  at  $\mathbf{Q} = [0.6, 0.6, 6.6]$  and  $T = 600$  K, computed using  $S_{ib}^o$ . For direct comparison, the INS instrumental energy resolution (ER) is accounted for in the solid curves [59]. The  $q$ -voxel dimensions used in both the measurement and computation are 0.075, 0.2, and 0.2 reciprocal lattice units along the  $[L, L, L]$ ,  $[0, 0, L]$ , and  $[-H, H, 0]$  directions, respectively.

cubic phonon interactions computed using DFT +  $U$  and the bubble diagram used to evaluate the self-energy are sufficient to describe experiment at  $T = 600$  K. We reevaluated Fig. 2 using  $S_{ib}^{HF}$  and  $S_{ib}^{QP}$ , while accounting for thermal expansion, and the net changes are found to be modest at  $T = 600$  K (see Sec. VIII in SM [15]).

The thermal conductivity will first be explored at up to  $T = 1400$  K using bare perturbation theory [see Fig. 3(a)], where the imaginary parts of the bubble and sunset diagrams will be considered. Recall that we are not accounting for magnons, defects, or boundary effects, and thus our results will not describe experiment below  $T \approx 400$  K. The  $S_{ib}^o$  BTE results using the imaginary part of the bubble diagram are reasonable above  $T = 400$  K as compared to experiment [4–7]. This favorable agreement is anticipated from our preceding favorable comparison with INS. However, the result systematically underpredicts experiment at high temperatures, and therefore it is compelling to include the quartic phonon interactions. We begin by using the imaginary parts of both the bare bubble and

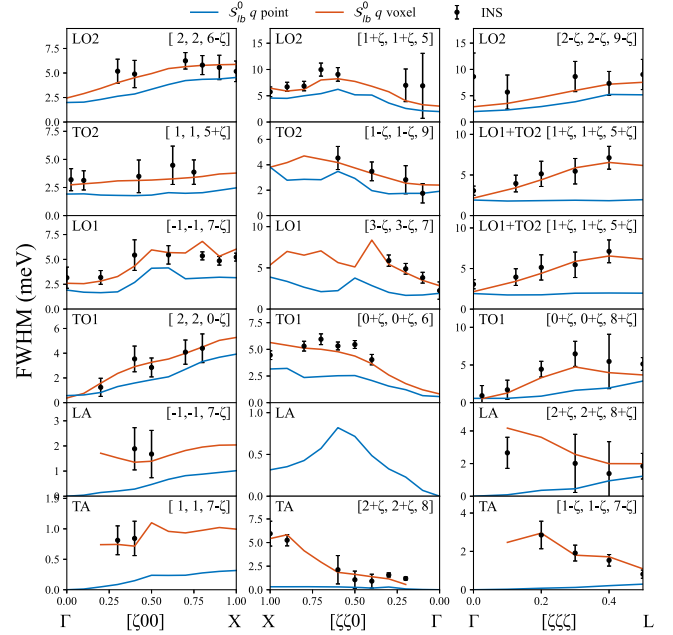


FIG. 2. FWHMs of the  $S(\mathbf{Q}, \omega)$  peaks as a function of  $q$  in various zones for  $\text{UO}_2$  at  $T = 600$  K. The  $S_{ib}^o$   $q$ -point and  $q$ -voxel results are shown as blue and red curves, respectively. INS results are shown as black points.

sunset diagrams ( $S_{bs}^o$ ), where the latter purely uses quartic interactions, and the result is pushed further away from experiment by a small amount. This same effect was previously observed in Ref. [14] (see SM [15], Fig. S1), though the value of their results are strongly underpredicted relative to our own (see Sec. II in SM [15]). Interestingly, above room temperature, roughly 30% of the thermal conductivity arises from phonon modes with energies above 26 meV, which are predominantly optical modes, and therefore the optical modes do play a nontrivial role in thermal transport (see Sec. VI in SM [15]). We proceed by including interband phonon contributions via the WTE, which increases the thermal conductivity monotonically with temperature, yielding good agreement with experiment. At  $T = 1400$  K, the interband portion contributes about 30% of the total thermal conductivity, which is nontrivial.

While the current approximation yields reasonable agreement with experiment, it is important to use a logically consistent approach where the real portion of the self-energy is not discarded and the effects of thermal expansion are included [see Fig. 3(b)]. When thermal expansion is included in the thermal conductivity calculation, a nontrivial decrease in thermal conductivity is observed: at  $T = 1400$  K, the decrease of the  $S_{bs}^o$  BTE result due to thermal expansion is nearly 50%. This strong decrease may explain the relatively low predicted thermal conductivity in Ref. [58], which used  $S_{ib}^o$  BTE and included thermal expansion. While the

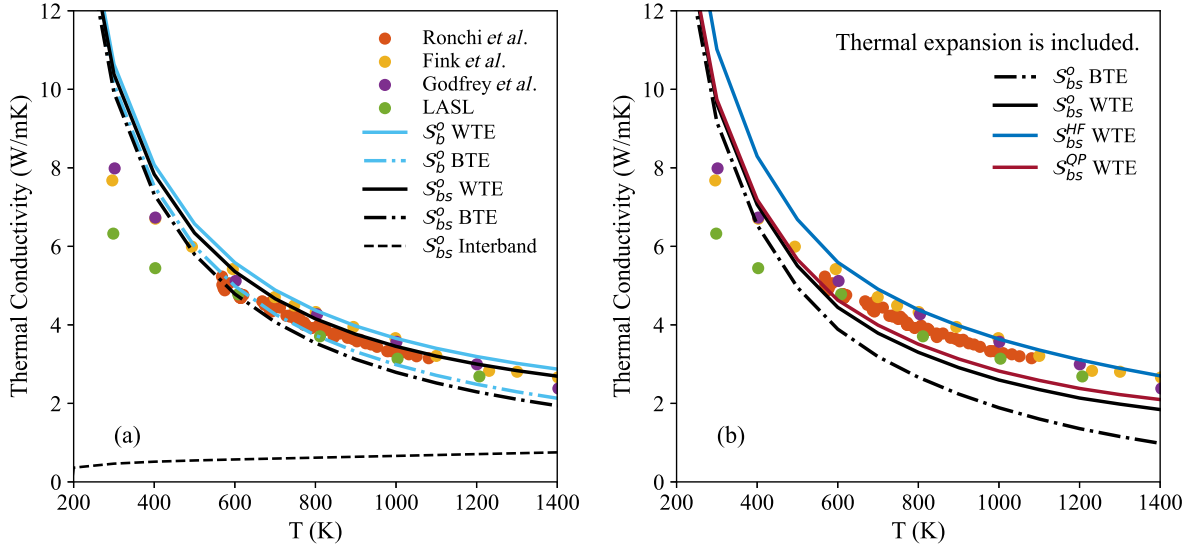


FIG. 3. Thermal conductivity computed using GGA +  $U$  + SOC ( $U = 4$  eV) and comparing with experiments [4–7]. Panel (a) presents the bare perturbation theory results without including thermal expansion. Panel (b) presents the results with thermal expansion and self-consistent perturbation theory.

interband contribution contained in the  $S_{bs}^o$  WTE result increases the predicted value, the thermal conductivity is still underpredicted as compared to experiment. However, it is still necessary to account for the real part of the phonon self-energy, and explore the possibility of accounting for higher order diagrams via self-consistent perturbation theory [43].

Nominally, we would expect the QP result to be better than HF as it sums additional diagrams, which are known to be relevant [43]. We first consider  $S_{bs}^{HF}$  WTE, which notably increases the thermal conductivity at high temperatures. This result is anticipated, given that the HF approximation nominally increases the effective harmonic frequencies, decreasing the phonon lifetime contribution from the bubble. The  $S_{bs}^{QP}$  WTE result is shifted downward from the HF result, slightly above the bare perturbation theory result using the bubble and sunset diagrams. The underestimation of the experimental thermal conductivity by  $S_{bs}^{QP}$  might be accounted for by including more diagrams, possibly requiring diagrams with phonon interactions beyond fourth order. Ideally, one would sum all possible diagrams and obtain the exact phonon self-energy, which can be done in the classical limit using molecular dynamics [43]. Another possibility for the discrepancy is that the Perdew, Burke, and Ernzerhof exchange correlation functional is not sufficiently describing the phonon interactions.

In summary, we have computed the scattering function and thermal conductivity of  $UO_2$  from first principles using various levels of self-consistent perturbation theory and compared to our own INS experiments and existing thermal conductivity experiments. The relevant contributions of this work include accurately describing the phonon interactions

in  $UO_2$  from first principles and illustrating the effects of improving the quality of the single particle phonon Green's function on the thermal conductivity. Favorable agreement between our theory and INS experiment is obtained for the FWHM of the scattering function across the Brillouin zone. In terms of quantitatively computing the thermal conductivity at high temperatures, we find that thermal expansion decreases the thermal conductivity while interband transitions increases the thermal conductivity, and these effects are of similar magnitude. Including quartic phonon interactions at the level of the bare sunset diagram causes a small decrease in thermal conductivity, while the self-consistent perturbation theory yielded moderate and appreciable increases for the quasiparticle and Hartree-Fock procedures, respectively. Aside from low temperatures where magnons and defects play important roles, phonon thermal transport in  $UO_2$  is now well characterized from first principles.

This work is supported by the Center for Thermal Energy Transport under Irradiation, an Energy Frontier Research Center funded by the U.S. Department of Energy (DOE) Office of Basic Energy Sciences. This research used resources at the Spallation Neutron Source, a DOE Office of Science User Facility operated by the ORNL. This research made use of Idaho National Laboratory computing resources, which are supported by the DOE Office of Nuclear Energy and the Nuclear Science User Facilities under Contract No. DE-AC07-05ID14517. This research also used resources of the National Energy Research Scientific Computing Center, a DOE Office of Science User Facility supported by the Office of Science of the U.S. Department of Energy under

Contract No. DE-AC02-05CH11231. The unfolding of phonons and phonon interactions was supported by Grant No. DE-SC0016507 funded by the U.S. Department of Energy, Office of Science.

- 
- [1] G. H. Lander and R. Caciuffo, *J. Phys. Condens. Matter* **32**, 374001 (2020).
- [2] D. H. Hurley, A. El-Azab, M. S. Bryan, M. W. D. Cooper, C. A. Dennett, K. Gofryk, L. He, M. Khafizov, G. H. Lander, M. E. Manley, J. M. Mann, C. A. Marianetti, K. Rickert, F. A. Selim, M. R. Tonks, and J. P. Wharry, *Chem. Rev.* **122**, 3711 (2022).
- [3] K. Gofryk, S. Du, C. R. Stanek, J. C. Lashley, X.-Y. Liu, R. K. Schulze, J. L. Smith, D. J. Safarik, D. D. Byler, K. J. McClellan, B. P. Uberuaga, B. L. Scott, and D. A. Andersson, *Nat. Commun.* **5**, 4551 (2014).
- [4] J. K. Fink, *J. Nucl. Mater.* **279**, 1 (2000).
- [5] J. L. Bates, *Nucl. Sci. Eng.* **21**, 26 (1965).
- [6] T. G. Godfrey, W. Fulkerson, T. G. Kollie, J. P. Moore, and D. L. McElroy, *J. Am. Ceram. Soc.* **48**, 297 (1965).
- [7] C. Ronchi, M. Sheindlin, D. Staicu, and M. Kinoshita, *J. Nucl. Mater.* **327**, 58 (2004).
- [8] Q. Yin and S. Y. Savrasov, *Phys. Rev. Lett.* **100**, 225504 (2008).
- [9] G. Kaur, P. Panigrahi, and M. C. Valsakumar, *Model. Simul. Mater. Sci. Eng.* **21**, 065014 (2013).
- [10] Z.-G. Mei, M. Stan, and J. Yang, *J. Alloys Compd.* **603**, 282 (2014).
- [11] B.-T. Wang, J.-J. Zheng, X. Qu, W.-D. Li, and P. Zhang, *J. Alloys Compd.* **628**, 267 (2015).
- [12] E. Torres and T. P. Kaloni, *J. Nucl. Mater.* **521**, 137 (2019).
- [13] E. Torres, I. CheikNjifon, T. P. Kaloni, and J. Pencer, *Comput. Mater. Sci.* **177**, 109594 (2020).
- [14] X. Yang, J. Tiwari, and T. Feng, *Mater. Today Phys.* **24**, 100689 (2022).
- [15] See Supplemental Materials at <http://link.aps.org/supplemental/10.1103/PhysRevLett.132.106502> for information about previous DFT +  $U$  studies on thermal conductivity of  $\text{UO}_2$ , the computational details and results of thermal conductivity, and the values of computed irreducible derivatives in this work. See also Refs. [16–25].
- [16] B.-T. Wang, P. Zhang, R. Lizárraga, I. Di Marco, and O. Eriksson, *Phys. Rev. B* **88**, 104107 (2013).
- [17] X. Gonze and C. Lee, *Phys. Rev. B* **55**, 10355 (1997).
- [18] M. A. Mathis, A. Khanolkar, L. Fu, M. S. Bryan, C. A. Dennett, K. Rickert, J. M. Mann, B. Winn, D. L. Abernathy, M. E. Manley, D. H. Hurley, and C. A. Marianetti, *Phys. Rev. B* **106**, 014314 (2022).
- [19] M. Idiri, T. Le Bihan, S. Heathman, and J. Rebizant, *Phys. Rev. B* **70**, 014113 (2004).
- [20] P. Santini, S. Carretta, G. Amoretti, R. Caciuffo, N. Magnani, and G. H. Lander, *Rev. Mod. Phys.* **81**, 807 (2009).
- [21] M. S. Bryan, J. W. L. Pang, B. C. Larson, A. Chernatynskiy, D. L. Abernathy, K. Gofryk, and M. E. Manley, *Phys. Rev. Mater.* **3**, 065405 (2019).
- [22] I. A. E. Agency, *Thermodynamic and transport properties of uranium dioxide and related phases* (1965), [https://inis.iaea.org/collection/NCLCollectionStore/\\_Public/24/071/24071477.pdf](https://inis.iaea.org/collection/NCLCollectionStore/_Public/24/071/24071477.pdf).
- [23] C. Ronchi, M. Sheindlin, M. Musella, and G. J. Hyland, *J. Appl. Phys.* **85**, 776 (1999).
- [24] H. Kim, M. H. Kim, and M. Kaviani, *J. Appl. Phys.* **115**, 123510 (2014).
- [25] T. R. Pavlov, M. R. Wenman, L. Vlahovic, D. Robba, R. J. M. Konings, P. Van Uffelen, and R. W. Grimes, *Acta Mater.* **139**, 138 (2017).
- [26] B. Dorado, B. Amadon, M. Freyss, and M. Bertolus, *Phys. Rev. B* **79**, 235125 (2009).
- [27] B. Amadon, F. Jollet, and M. Torrent, *Phys. Rev. B* **77**, 155104 (2008).
- [28] G. Jomard, B. Amadon, F. Bottin, and M. Torrent, *Phys. Rev. B* **78**, 075125 (2008).
- [29] F. Zhou and V. Ozoliņš, *Phys. Rev. B* **83**, 085106 (2011).
- [30] S. Zhou, H. Ma, E. Xiao, K. Gofryk, C. Jiang, M. E. Manley, D. H. Hurley, and C. A. Marianetti, *Phys. Rev. B* **106**, 125134 (2022).
- [31] D. A. Broido, A. Ward, and N. Mingo, *Phys. Rev. B* **72**, 014308 (2005).
- [32] D. A. Broido, M. Malorny, G. Birner, N. Mingo, and D. A. Stewart, *Appl. Phys. Lett.* **91**, 231922 (2007).
- [33] D. A. Broido, L. Lindsay, and A. Ward, *Phys. Rev. B* **86**, 115203 (2012).
- [34] L. Chaput, *Phys. Rev. Lett.* **110**, 265506 (2013).
- [35] W. Li, J. Carrete, N. A. Katcho, and N. Mingo, *Comput. Phys. Commun.* **185**, 1747 (2014).
- [36] T. Tadano, Y. Gohda, and S. Tsuneyuki, *J. Phys. Condens. Matter* **26**, 225402 (2014).
- [37] A. Togo, L. Chaput, and I. Tanaka, *Phys. Rev. B* **91**, 094306 (2015).
- [38] A. Chernatynskiy and S. R. Phillpot, *Comput. Phys. Commun.* **192**, 196 (2015).
- [39] T. Feng and X. Ruan, *Phys. Rev. B* **93**, 045202 (2016).
- [40] T. Feng, L. Lindsay, and X. Ruan, *Phys. Rev. B* **96**, 161201 (R) (2017).
- [41] M. Simoncelli, N. Marzari, and F. Mauri, *Nat. Phys.* **15**, 809 (2019).
- [42] M. Simoncelli, N. Marzari, and F. Mauri, *Phys. Rev. X* **12**, 041011 (2022).
- [43] E. Xiao and C. A. Marianetti, *Phys. Rev. B* **107**, 094303 (2023).
- [44] V. I. Anisimov, F. Aryasetiawan, and A. I. Lichtenstein, *J. Phys. Condens. Matter* **9**, 767 (1997).
- [45] D. Hooton, *London, Edinburgh, Dublin Phil. Mag. J. Sci.* **46**, 422 (1955).
- [46] E. Xiao, H. Ma, M. S. Bryan, L. Fu, J. M. Mann, B. Winn, D. L. Abernathy, R. P. Hermann, A. R. Khanolkar, C. A. Dennett, D. H. Hurley, M. E. Manley, and C. A. Marianetti, *Phys. Rev. B* **106**, 144310 (2022).
- [47] Y.-Y. Qi, T. Zhang, Y. Cheng, X.-R. Chen, D.-Q. Wei, and L.-C. Cai, *J. Appl. Phys.* **119**, 095103 (2016).
- [48] A. C. Momin, E. B. Mirza, and M. D. Mathews, *J. Nucl. Mater.* **185**, 308 (1991).

- [49] P. E. Blöchl, *Phys. Rev. B* **50**, 17953 (1994).
- [50] G. Kresse and D. Joubert, *Phys. Rev. B* **59**, 1758 (1999).
- [51] G. Kresse and J. Hafner, *Phys. Rev. B* **47**, 558 (1993).
- [52] G. Kresse and J. Furthmüller, *Phys. Rev. B* **54**, 11169 (1996).
- [53] J. P. Perdew, K. Burke, and M. Ernzerhof, *Phys. Rev. Lett.* **77**, 3865 (1996).
- [54] S. L. Dudarev, G. A. Botton, S. Y. Savrasov, C. J. Humphreys, and A. P. Sutton, *Phys. Rev. B* **57**, 1505 (1998).
- [55] L. Fu, M. Kornbluth, Z. Cheng, and C. A. Marianetti, *Phys. Rev. B* **100**, 014303 (2019).
- [56] J. Y. Lin, A. Banerjee, F. Islam, M. D. Le, and D. L. Abernathy, *Physica (Amsterdam)* **562B**, 26 (2019).
- [57] M. S. Bryan, L. Fu, K. Rickert, D. Turner, T. A. Prusnick, J. M. Mann, D. L. Abernathy, C. A. Marianetti, and M. E. Manley, *Commun. Phys.* **3**, 1 (2020).
- [58] J. W. L. Pang, W. J. L. Buyers, A. Chernatynskiy, M. D. Lumsden, B. C. Larson, and S. R. Phillpot, *Phys. Rev. Lett.* **110**, 157401 (2013).
- [59] D. L. Abernathy, M. B. Stone, M. Loguillo, M. Lucas, O. Delaire, X. Tang, J. Lin, and B. Fultz, *Rev. Sci. Instrum.* **83**, 015114 (2012).